BIOCHEMISTRY
including biophysical chemistry & molecular biology

Article

pubs.acs.org/biochemistry

NMR Structure of the Human Rad18 Zinc Finger in Complex with Ubiquitin Defines a Class of UBZ Domains in Proteins Linked to the DNA Damage Response

Alessandro A. Rizzo, Paige E. Salerno, Irina Bezsonova, and Dmitry M. Korzhnev*

Department of Molecular Biology and Biophysics, University of Connecticut Health Center, Farmington, Connecticut 06030, United States

Supporting Information

ABSTRACT: Ubiquitin-mediated interactions are critical for the cellular DNA damage response (DDR). Therefore, many DDR-related proteins contain ubiquitin-binding domains, including ubiquitin-binding zinc fingers (UBZs). The majority of these UBZ domains belong to the C_2H_2 (type 3 Polη-like) or C_2HC (type 4 Rad18-like) family. We have used nuclear magnetic resonance (NMR) spectroscopy to characterize the binding to ubiquitin and determine the structure of the type 4 UBZ domain (UBZ4) from human Rad18, which is a key ubiquitin ligase in the DNA damage tolerance pathway responsible for monoubiquitination of the DNA sliding clamp PCNA. The Rad18-UBZ domain binds ubiquitin with micromolar affinity and adopts a $\beta1-\beta2-\alpha$ fold similar to the previously characterized type 3 UBZ domain (UBZ3) from the translesion synthesis DNA polymerase Polη. However, despite nearly identical structures, a disparity in the location of binding-induced NMR chemical shift perturbations shows that the Rad18-UBZ4 and Polη-UBZ3 domains bind ubiquitin in distinctly different modes. The Rad18-UBZ4 domain interacts with ubiquitin with the α-helix and strand $\beta1$ as shown by the structure of the Rad18-UBZ domain−ubiquitin complex determined in this work, while the Polη-UBZ3 domain exclusively utilizes the α-helix. Our findings suggest the existence of two classes of UBZ domains in DDR-related proteins with similar structures but unique ubiquitin binding properties and provide context for further study to establish the differential roles of these domains in the complex cellular response to DNA damage.

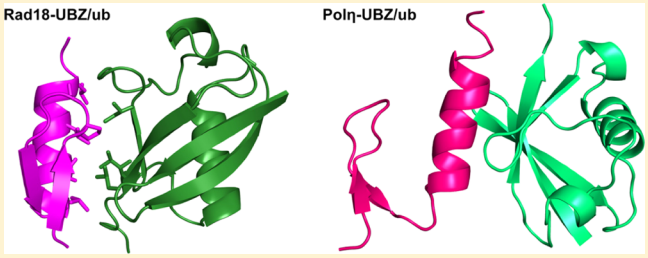

Maintenance of genome integrity and faithful DNA replication are critical for the survival of all forms of life. Working against this are numerous genotoxic agents from endogenous or exogenous sources that constantly modify the chemical structure of DNA and chromatin. Common types of DNA damage include UV-induced thymine-thymine dimers, N2-guanine adducts formed by benzo[*a*]pyrene contained in smoke, double-strand breaks (DSBs) caused by ionizing radiation, and many others. Such varied types of damage require living organisms to possess complex and dynamic DNA damage response (DDR) pathways.[1]

DDR pathways are activated by a cascade of signaling events mediated by protein post-translational modifications and regulated by a network of molecular interactions that can be quickly tuned in response to the type of damage.[1−8] Separate from its function in protein degradation,[9] protein ubiquitination plays a critical signaling role in the DDR.[3,5−7,10−14] For example, Rad6/Rad18-dependent monoubiquitination of the DNA sliding β-clamp PCNA in response to DNA damage signals switching from normal DNA replication to translesion synthesis (TLS), a process conducted by specialized low-fidelity DNA polymerases.[5,6,15−19] These mutagenic TLS enzymes can bypass replication blocks that stem from the inability of spatially constricted active sites of high-fidelity replicative DNA polymerases to accommodate most types of DNA lesions.[17,18,20,21] Subsequent polyubiquitination of PCNA via the formation of K63-linked ubiquitin chains signals an error-free DNA damage tolerance pathway that utilizes a template switching mechanism.[2,22−24] To respond to these ubiquitin signals, DDR-related proteins often contain ubiquitin-binding modules such as ubiquitin-binding motifs (UBMs) and ubiquitin-binding zinc fingers (UBZs) found in TLS DNA polymerases.[5,10,12,14,25,26]

Rad18 is an E3 ubiquitin-protein ligase central to the DDR,[5,6,10−12] which, along with a RING domain, a DNA-binding SAP domain, and other modules, possesses a ubiquitin-binding C_2HC UBZ domain.[25,27] Rad18 functions in at least two ubiquitin-dependent branches of the DDR, translesion synthesis (TLS) and homologous recombination repair (HRR).[2,5,6,10,11,28] The role of Rad18 in translesion synthesis (TLS) is well-documented.[2,5,6,10,28,29] Rad18-dependent ubiquitination of PCNA is a signal for activation of TLS presumably by increasing the affinity of TLS DNA polymerases that contain ubiquitin-binding domains for PCNA.[2,5,6,10,28,29] Functionally,

Received: July 4, 2014
Revised: August 27, 2014
Published: August 27, 2014

   dx.doi.org/10.1021/bi500823h | *Biochemistry* 2014, 53, 5895−5906

Rad18 knockout was shown to sensitize cells to the types of DNA damage that can be bypassed by TLS.[29] However, the role of the Rad18-UBZ domain in PCNA ubiquitination and TLS, if any, is unclear, because deletion of the UBZ domain has no effect on PCNA ubiquitination or cell survival after UV-induced DNA damage *in vivo*.[11,30,31]

Separate from its role in PCNA ubiquitination and TLS, Rad18 was shown to localize to DSBs and recruit Rad51c for initiation of homologous recombination repair (HRR).[11,32,33] In a Rad18 construct lacking the UBZ domain, or with a mutant that disrupts a zinc coordination site (C207F), localization to DSB sites after treatment with ionizing radiation or camptothecin was abolished.[11,32] In addition, a construct of the Rad18-UBZ domain fused to a nuclear localization signal (NLS) was able to localize to DSBs after treatment, showing that the UBZ (with NLS) is both sufficient and necessary for targeting Rad18 to DSB sites.[11] Overall, these findings suggest that the Rad18-UBZ domain functions primarily in the HRR signaling cascade rather than in PCNA ubiquitination and TLS activation.

UBZ domains are found in many DDR-linked proteins such as Rad18, Polη, Polκ, Wrnip1, FAN1, and others.[12,14,25,26] Members of the UBZ class of ubiquitin-binding zinc fingers share many conserved residues, including an invariant aspartate that is necessary for ubiquitin binding (D221 in Rad18).[25,33,34] However, sequence alignment of UBZ domains has led to a distinction between the type 3 C_2H_2 domain found in TLS DNA polymerase Polη (UBZ3) and the type 4 C_2HC domain found in Rad18 (UBZ4).[14,25,34] The NMR structure of the Polη-UBZ3 domain (PDB entry 2I5O) has shown that the domain adopts a classical $\beta1-\beta2-\alpha$ fold usually seen in DNA-binding zinc fingers.[35,36] Using NMR chemical shift perturbations and spin labeling, the Polη-UBZ3 domain was shown to bind ubiquitin on a hydrophobic patch located on the outer edge of the UBZ α-helix in a manner similar to the MIU/IUIM (motif interacting with ubiquitin/inverted ubiquitin-interacting motif).[35,37] This mode of ubiquitin binding was also reported for the UBZ domain from NEMO.[38]

Here, we have used NMR spectroscopy to study the binding of the type 4 Rad18-UBZ domain to ubiquitin and to determine the structure of the Rad18-UBZ4 domain in isolation and in complex with ubiquitin. The Rad18-UBZ4 domain has the same $\beta1-\beta2-\alpha$ topology as the Polη-UBZ3 domain yet binds ubiquitin using a different interface. This comparison of the Polη-UBZ3 and Rad18-UBZ4 domains, therefore, defines two classes of UBZ domains with nearly identical structures, but different ubiquitin-binding modes, providing context for further study of their diverging functions.

EXPERIMENTAL PROCEDURES

Protein Sample Preparation for NMR Spectroscopy. The gene encoding the UBZ domain from human Rad18 (residues 186−244) was previously cloned into a pDEST vector with a GST affinity tag (courtesy of K. Cimprich). This construct was used to design a shorter UBZ domain construct comprised of residues 198−227 that was used in our structural and ubiquitin binding studies. Point mutations and deletions in the Rad18-UBZ gene were introduced by standard site-directed mutagenesis protocols[39] using Q5 DNA polymerase (New England Biolabs) and confirmed by sequencing (Genewiz).

Protein was expressed in *Escherichia coli* BL21(DE3) cells transformed with the Rad18-UBZ plasmid grown to an OD_{600} of 0.8 at 37 °C followed by induction of protein expression at 24 °C overnight using 1 mM IPTG. The unlabeled protein was expressed in LB medium, while for isotopic labeling, cells were grown in M9 medium containing 1 g/L $^{15}NH_4Cl$ and 4 g/L [$^{12}C_6$]glucose or 2 g/L [$^{13}C_6$]glucose. One hour before induction, the M9 medium was brought to 100 μM $ZnCl_2$. Cells were harvested by centrifugation, resuspended in lysis buffer containing 10 mM Na_2HPO_4, 1.8 mM KH_2PO_4, 140 mM NaCl, and 10 μM PMSF (pH 8), and lysed by sonication. The lysate was clarified by centrifugation, and the supernatant was filtered through a 0.45 μm syringe filter, applied to a Glutathione Sepharose 4B column (GE Healthcare), and incubated for 30 min at 4 °C. After being extensively washed with lysis buffer, the GST-UBZ fusion was eluted with buffer containing 50 mM Tris base and 33 mM reduced glutathione (pH 7.5). The GST tag was cleaved by thrombin overnight at room temperature in elution buffer. The protein was concentrated using a 3.5 kDa cutoff Centricon (Millipore) and purified on a gel-filtration HiLoad 16/60 Superdex 75 column (GE Healthcare) using NMR buffer containing 25 mM MOPS-NaOH, 50 mM NaCl, and 50 μM $ZnCl_2$ (pH 6.5). All NMR experiments were conducted in this NMR buffer after dilution to include 10% ^2H_2O.

Ubiquitin was purified by the same general protocol with the following exceptions. Ubiquitin was expressed from pET15b with an N-terminal His_6 tag and purified on HisPur Ni-NTA resin (Thermo Scientific). The His_6 tag was cleaved by thrombin overnight at room temperature, while the protein was dialyzed (2 times) against 2 L of 20 mM Tris-HCl, 100 mM NaCl buffer (pH 8.4). The ubiquitin was then purified on the HiLoad 16/60 Superdex 75 column (GE Healthcare) using the MOPS NMR buffer described above.

NMR Resonance Assignment and Structure Calculation. NMR spectra for resonance assignment and structure calculation of the human Rad18-UBZ domain (residues 198−227) and its complex with ubiquitin were collected at 25 °C on 600 and 800 MHz (^1H) Agilent VNMRS spectrometers equipped with cold probes. The backbone and side-chain resonance assignments for (i) the $^{15}N/^{13}C$-labeled UBZ domain, (ii) the $^{15}N/^{13}C$-labeled UBZ domain saturated with unlabeled ubiquitin, and (iii) $^{15}N/^{13}C$-labeled ubiquitin saturated with unlabeled UBZ domain were performed using two-dimensional $^1H-^{15}N$ HSQC and $^1H-^{13}C$ HSQC and 3D HNCACB, HNCO, HBHA(CO)NH, HC(C)H-TOCSY, and (H)CCH-TOCSY spectra.[40] The intramolecular $^1H-^1H$ distance restraints for structure calculation of the free UBZ domain and the UBZ domain−ubiquitin complex were derived from 3D ^{15}N- and ^{13}C-edited NOESY-HSQC spectra (mixing time of 150 ms),[40] while intermolecular distance restraints for the UBZ−ubiquitin complex were obtained from 3D ^{13}C-edited, ^{15}N,^{13}C-filtered NOESY-HSQC spectra[41] recorded for both $^{15}N/^{13}C$-labeled UBZ−unlabeled ubiquitin and $^{15}N/^{13}C$-labeled ubiquitin−unlabeled UBZ pairs. Spectra were processed with NMRPipe,[42] and the backbone and side-chain assignments were performed using CCPNmr Analysis.[43] Note that initial NMR experiments collected on the original Rad18-UBZ construct (residues 186−244) revealed that this construct has extensive unstructured N- and C-termini (confirmed by a $^{15}N\{^1H\}$NOE experiment[44]), which led us to the generation of a construct composed of residues 198−227 with shorter disordered tails beyond the structured Rad18-UBZ domain.

Structure calculation of the free UBZ domain was performed in CYANA 2.1[45] using fully automated NOESY assignment. Distance restraints were generated and calibrated automatically

Table 1. Summary of NMR-Derived Restraints Used for Structure Calculation of the Free UBZ Domain and the UBZ Domain−Ubiquitin Complex and Structure Refinement Statistics Based on the 20 Lowest-Energy Models

	free UBZ domain/UBZ domain−ubiquitin complex
experimental restraints	
total no. of restraints	799/2723
total no. of NOE-based distance restraints	706/2429
long-range ($\|i - j\| \geq 5$)	207/827
medium-range ($1 < \|i - j\| < 5$)	158/498
sequential	212/645
intraresidue	129/459
intermolecular	−/100
no. of ϕ/ψ dihedral angle restraints	47/167
no. of zinc restraints	22/22
no. of hydrogen bond restraints	24/105
rmsd from ideal geometry	
bonds (Å)	0.015 ± 0.0003/0.014 ± 0.0002
angles (deg)	1.037 ± 0.032/0.096 ± 0.013
rmsd from experimental restraints	
NOE distances (Å)	0.025 ± 0.002/0.021 ± 0.001
dihedrals (deg)	0.644 ± 0.117/0.551 ± 0.068
rmsd from mean structure[a]	
backbone atoms (Å)	0.17 ± 0.04/0.34 ± 0.06
heavy atoms (Å)	0.44 ± 0.06/0.65 ± 0.05
Ramachandran plot, Procheck[a]	
most favored (%)	97.9/86.7
additionally allowed (%)	2.1/13.3
generously allowed (%)	0.0/0.1
disallowed (%)	0.0/0.0

[a]Calculated over structured residues 201−224, and 201−224 and 1−74, using the iCing online server.[66]

by CYANA using manually picked ^{15}N- and ^{13}C-edited NOESY-HSQC peak lists. The restraints for backbone dihedral angles were determined using TALOS+.[46] Additional restraints were introduced for distances between the zinc ion and zinc-coordinating atoms to enforce the tetrahedral geometry of the zinc center.[47] After an initial round of structure calculations of the free UBZ domain, hydrogen bond restraints were added on the basis of NOE analysis, the structure was recalculated, and the 20 lowest-energy structures were refined in explicit water with CNS.[48] The generation of the structure of the Rad18-UBZ domain−ubiquitin complex was performed in a similar manner in CYANA 2.1,[45] using intramolecular distance restraints derived from ^{15}N- and ^{13}C-edited NOESY-HSQC spectra for both the UBZ domain and ubiquitin and intermolecular distance restraints obtained from the two ^{13}C,^{15}N-filtered NOESY-HSQC spectra.[41] The 20 lowest-energy structures of the complex were refined in explicit water using CNS.[48] The summary of restraints used in the structure calculations of the Rad18-UBZ domain and the Rad18-UBZ domain−ubiquitin complex and structural statistics are listed in Table 1.

NMR Titration Experiments. To study the interaction of the Rad18-UBZ domain with ubiquitin, we have performed NMR binding experiments in which 50 μM ^{15}N-labeled wild-type (WT) or D221A UBZ domain was titrated with increasing amounts of 1.9 mM unlabeled ubiquitin (to a maximal 4:1 ubiquitin:UBZ ratio) and reciprocal experiments in which 50 μM ^{15}N-labeled ubiquitin was titrated with 1.8 (1.5) mM unlabeled WT (D221A) UBZ domain stocks (up to a 4:1 UBZ:ubiquitin ratio). The UBZ construct used for titrations contained residues 198−227. The binding was monitored by ^{1}H−^{15}N HSQC spectra collected on a 500 or 600 MHz Agilent VNMRS spectrometer at 25 °C at each point of the titration. The titrations revealed gradual movement for a number of peaks in the Rad18-UBZ domain and ubiquitin spectra toward their positions in the complex indicative of fast (on the NMR time scale) exchange between the free and bound forms of the proteins.

For each titration series, the dissociation constant (K_d) for the complex was calculated from a least-squares fit of the cumulative chemical shift change ($\Delta\omega_{obs}$) for the backbone amide groups in the ^{15}N-labeled protein (P) upon its titration with the unlabeled ligand (L) to the following equations:

$$\Delta\omega_{obs} = \Delta\omega\frac{L_0 - [L]}{P_0} \quad (1)$$

$$[L] = \frac{1}{2}\left[\sqrt{(P_0 - L_0 + K_d)^2 + 4L_0K_D} - (P_0 - L_0 + K_d)\right] \quad (2)$$

where $\Delta\omega_{obs}$ is a sum of binding-induced chemical shift changes $\{[\Delta\omega_H^2 + (\gamma_N/\gamma_H\Delta\omega_N)^2]^{1/2}\}$ for all nonoverlapped backbone amide resonances, ω_H and ω_N are ^{1}H and ^{15}N chemical shift perturbations, respectively, γ_H and γ_N are ^{1}H and ^{15}N gyromagnetic ratios, respectively, $\Delta\omega$ is the cumulative chemical shift difference between the bound and free states, P_0 and L_0 are total protein and ligand concentrations, respectively, and [L] is the concentration of the free ligand. The chemical shift differences between the bound and free states for individual backbone amide groups ($\Delta\omega_i$) were then calculated from fits of the per-residue titration profiles with the K_d fixed to the previously determined values.

Note that the dissociation constants extracted from the NMR titration data are sensitive to systematic errors in the measured

dx.doi.org/10.1021/bi500823h | Biochemistry 2014, 53, 5895−5906

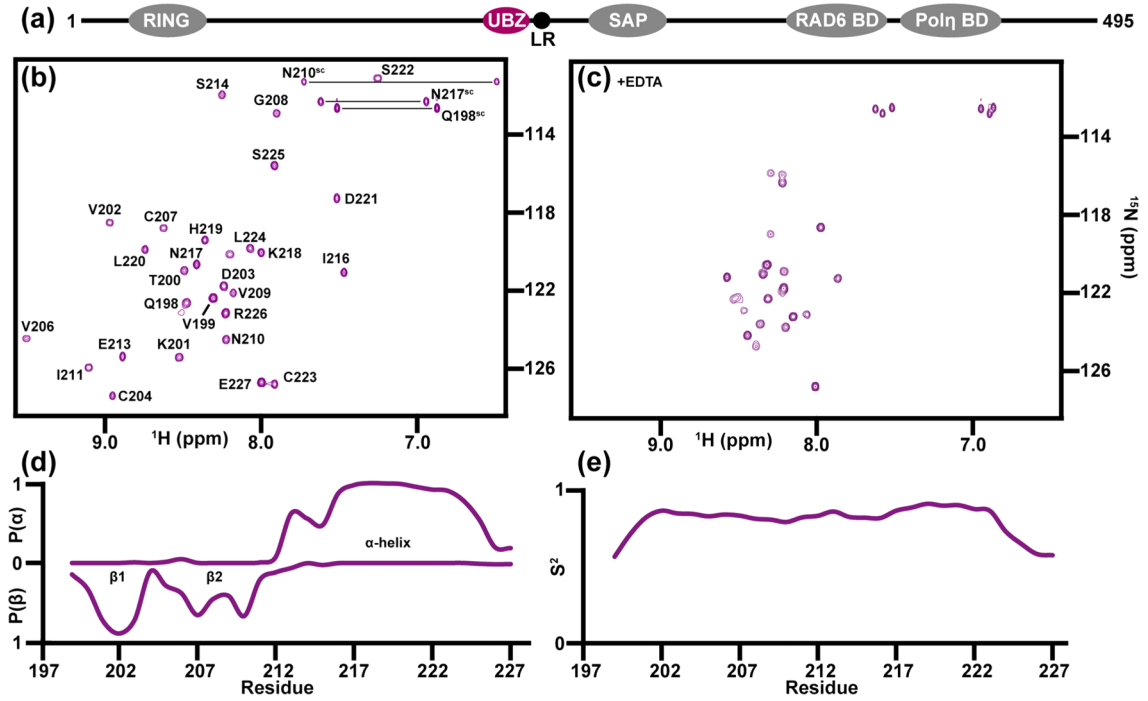

Figure 1. (a) Linear arrangement of domains in human Rad18.[27] (b and c) $^{1}H-^{15}N$ HSQC spectra of the Rad18-UBZ construct composed of residues 198−227 in the absence and presence, respectively, of 10 mM EDTA. (d) Probabilities of α-helix [$P(\alpha)$] and β-sheet [$P(\beta)$] predicted by TALOS+[46] plotted vs Rad18-UBZ domain residue number. (e) Order parameters (S^2) for the backbone amide groups of the Rad18-UBZ domain calculated in TALOS+[46] using the RCI approach.[56,57]

protein (P_0) and ligand (L_0) concentrations. For example, in our experimental setup, a hypothetical 20% overestimated concentration of the WT UBZ stocks with an accurate ubiquitin concentration could result a 2-fold stronger affinity for the complex obtained from the titration of the ^{15}N-Rad18-UBZ domain with the unlabeled ubiquitin, and 2-fold weaker affinity obtained from titration of ^{15}N-ubiquitin with the unlabeled Rad18-UBZ domain. In such a scenario, one would expect 4-fold different K_d values obtained from the two reciprocal titrations. Moderate errors in concentrations of both proteins could thus lead to significant deviations in K_d values measured in reciprocal titrations.

For our titration experiments, the concentrations of ubiquitin stocks were measured by UV−vis absorbance at 280 nm (A_{280}) of protein unfolded in 8 M GuHCl and validated by amino acid analysis (University of California at Davis Molecular Structure Facility), resulting in concentrations matching within 10%. Because of the small extinction coefficient of the Rad18-UBZ domain, it is not possible to accurately estimate its concentration from A_{280}. Therefore, the UBZ stock concentrations were measured by amino acid analysis only.

RESULTS AND DISCUSSION

Human Rad18 is a 495 amino acid E3 ubiquitin-protein ligase central to the cellular DNA damage response.[5,6,11,28,29] Figure 1 a shows a linear schematic illustrating the domain arrangement in human Rad18, including the N-terminal RING domain characteristic of E3 ubiquitin-protein ligases,[49] the ubiquitin-binding zinc finger (UBZ) followed by an LR motif,[50] the DNA-binding SAP domain, the binding domain for the ubiquitin-conjugating E2 enzyme Rad6 (Rad6BD), and the binding motif for the TLS DNA polymerase Polη (PolηBD).[27] The structures of the human Rad18-RING homodimer[51] and the Rad6 complex with the Rad18-Rad6BD domain[52] have been previously reported. Here, we complement these studies by structural characterization of the human Rad18-UBZ domain and its complex with ubiquitin.

NMR Structure of the Rad18-UBZ Domain. Initially, we expressed and purified a recombinant UBZ domain encompassing residues 186−244 from human Rad18. A $^{1}H-^{15}N$ HSQC spectrum of this construct displays a number of intense peaks in the random coil region originating from unstructured N- and C-terminal regions (data not shown). High flexibility in these residues was confirmed by a $^{15}N\{^{1}H\}$NOE experiment,[44] indicating that the structured part of the Rad18-UBZ domain consists of ∼25 residues with positive $^{15}N\{^{1}H\}$ NOE values. As a result, a shorter construct encompassing residues 198−227 was generated for further study, which includes all residues from the structured part of the UBZ domain but has shorter N- and C-terminal tails.

A $^{1}H-^{15}N$ HSQC spectrum of the Rad18-UBZ domain (residues 198−227) displays excellent peak dispersion, suggesting that this construct includes a structured and autonomously folding domain (Figure 1b). Similar to what has been shown for other zinc-binding domains,[53−55] the zinc ion plays a critical role in maintaining structural integrity of the Rad18-UBZ domain. In the presence of excess EDTA, the $^{1}H-^{15}N$ HSQC spectrum of the Rad18-UBZ domain assumes a distinctly random coil appearance, suggesting a complete unfolding of the domain (Figure 1c). After the NMR resonance assignments were completed, the backbone and C^{β} chemical shifts of the Rad18-UBZ domain were used to predict the secondary structure (Figure 1d) and backbone flexibility (Figure 1e) of the domain using TALOS+.[46] These data indicate the Rad18-UBZ domain has the classical $\beta1-\beta2-\alpha$ fold that is found in both DNA-binding zinc fingers[36] and the UBZ domain from the TLS DNA polymerase Polη[35] (Figure 1d). High order parameters (S^2) for the backbone amide

dx.doi.org/10.1021/bi500823h | Biochemistry 2014, 53, 5895−5906

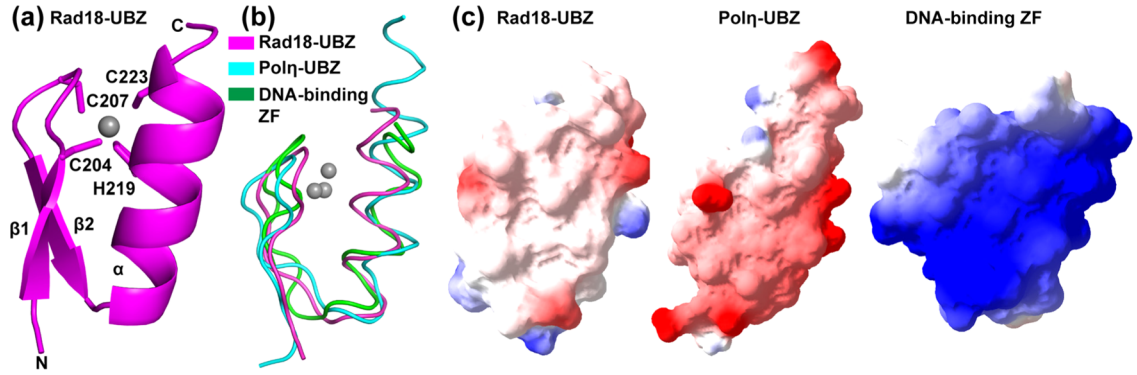

Figure 2. (a) NMR structure of the human Rad18-UBZ domain shown as a ribbon diagram with side chains of zinc-coordinating residues C204, C207, H219, and C223 displayed as sticks. (b) Overlay of the Rad18-UBZ domain (magenta) with the Polη-UBZ domain[35] (cyan) and a DNA-binding zinc finger from Xfin[36] (green). Compared to residues 200−225 on the Rad18-UBZ domain, the Polη-UBZ domain displays a backbone rmsd of 1.2 Å over residues 630−659 (excludes an additional helical turn at the C-terminus), and the DNA-binding zinc finger displays an rmsd of 0.82 Å over all residues. (c) Electrostatic charge distribution on the surface of strand β1 and the α-helix in the Rad18-UBZ domain (left), the Polη-UBZ domain (middle), and the Xfin zinc finger (right) generated using Swiss PDB viewer.[64] All molecules in plots a−c are shown in the same orientation.

groups predicted in TALOS+[46] using the Random Coil Index (RCI) approach[56,57] suggest that the Rad18-UBZ domain is highly ordered (Figure 1e; S^2 = 1 for fully constrained and S^2 = 0 for unconstrained angular motion of the N−H bond).

Figure 2a shows the structure of the Rad18-UBZ domain determined by solution NMR spectroscopy. The generated structural ensemble of the UBZ domain displays excellent agreement with the experimental restraints and minimal violations from idealized molecular geometry (Table 1). The domain adopts a classical β1−β2−α zinc finger fold with the α-helix (P212−L224) packed against the two antiparallel β-stands arranged in a short β-hairpin (K201−P212). The zinc ion is coordinated by residues C204 from strand β1, C207 from the β1−β2 loop, and H219 and C223 from the α-helix. The side chains of V206, I211, I216, and to some extent L220 form what little hydrophobic core is found in this domain.

Figure 2b shows an overlay of the UBZ domains from Rad18 and the TLS DNA polymerase Polη[35] with a DNA-binding zinc finger from the *Xenopus* protein Xfin.[36] Remarkably, these domains with distinctly different binding activities adopt nearly identical backbone folds. Figure 2c shows the electrostatic charge distribution on the surface of the UBZ domains and the DNA-binding zinc finger, suggesting that the binding preferences of the domains are determined by surface-exposed amino acid residues. Thus, the zinc finger from Xfin has a broad distribution of positively charged residues involved in DNA binding,[36] while the corresponding face of the UBZ domains formed by the α-helix and strand β1 is hydrophobic (Rad18-UBZ domain) or slightly negatively charged (Polη-UBZ domain) (Figure 2c). In comparing the Rad18-UBZ and Polη-UBZ domains, one may also notice that the α-helix in Polη, which is implicated in ubiquitin binding, is structured over additional C-terminal residues (Figure 2b).

Ubiquitin Binding by the Wild-Type and Mutant Rad18-UBZ Domains. Previous studies have established the ubiquitin binding activity of the Rad18-UBZ domain using pull-down assays[11,27] and surface plasmon resonance.[27,34] In this work, we have used NMR titration experiments to study the binding of the WT Rad18-UBZ domain to ubiquitin with amino acid resolution. Panels a and b of Figure 3 show the results of two reciprocal titrations in which the unlabeled ubiquitin stock was gradually added to a ^{15}N-labeled UBZ solution (plot a) and the unlabeled UBZ stock was added to a ^{15}N-labeled ubiquitin solution (plot b). ^{1}H−^{15}N HSQC spectra recorded at each step of the titrations (Figure 3a,b) display extensive binding-induced chemical shift perturbations for a number of amide resonances that confirm a specific interaction between the two proteins.

The binding-induced NMR chemical shift changes for both partners were quantified and analyzed to extract the dissociation constant (K_d) for the WT Rad18-UBZ domain−ubiquitin complex and per-residue chemical shift differences ($\Delta\omega_i$) between the bound and free states for the backbone amide groups. Panels c and d of Figure 3 show the normalized cumulative $^{1}H^{N}$ and ^{15}N chemical shift changes for non-overlapped amide resonances of the ^{15}N-labeled Rad18-UBZ domain (plot c) and ^{15}N-labeled ubiquitin (plot d) as a function of the concentration of added unlabeled partner (filled diamonds) and their best fits to the two-state binding model (lines). The extracted dissociation constants for the WT Rad18-UBZ domain−ubiquitin complex of 4.8−19.0 μM (25 °C) are in reasonable agreement with previously reported values of 38−42 μM obtained by surface plasmon resonance.[27,34] Note that somewhat different K_d values were extracted from the two reciprocal titrations, presumably because of systematic errors in the measured UBZ concentrations (see Experimental Procedures).

Rad18 constructs with mutations in the zinc finger domain have been utilized in previous *in vivo* and *in vitro* studies to gain insights into the role of this domain in Rad18 function.[11,27,30−32] One such mutation, C207F, disrupts one of the four zinc-coordinating residues of the domain. Rad18 was shown to localize to double-stranded DNA breaks (DSBs) in a UBZ-dependent manner and form ionizing radiation-induced foci that are thought to be repair complexes.[11] These foci are visible by fluorescence microscopy after treatment, but the Rad18 C207F mutant is able neither to form these foci nor to interact with another putative binding partner 53BP1.[11,32] A ^{1}H−^{15}N HSQC spectrum of the Rad18-UBZ domain in the presence of excess EDTA shows that the domain requires zinc for proper folding, because upon addition of EDTA the peaks clearly move to the random coil region of the spectrum (Figure 1c). These findings indicate that previous *in vivo* results using the C207F mutation that impairs the ability of the UBZ to

dx.doi.org/10.1021/bi500823h | *Biochemistry* 2014, 53, 5895−5906

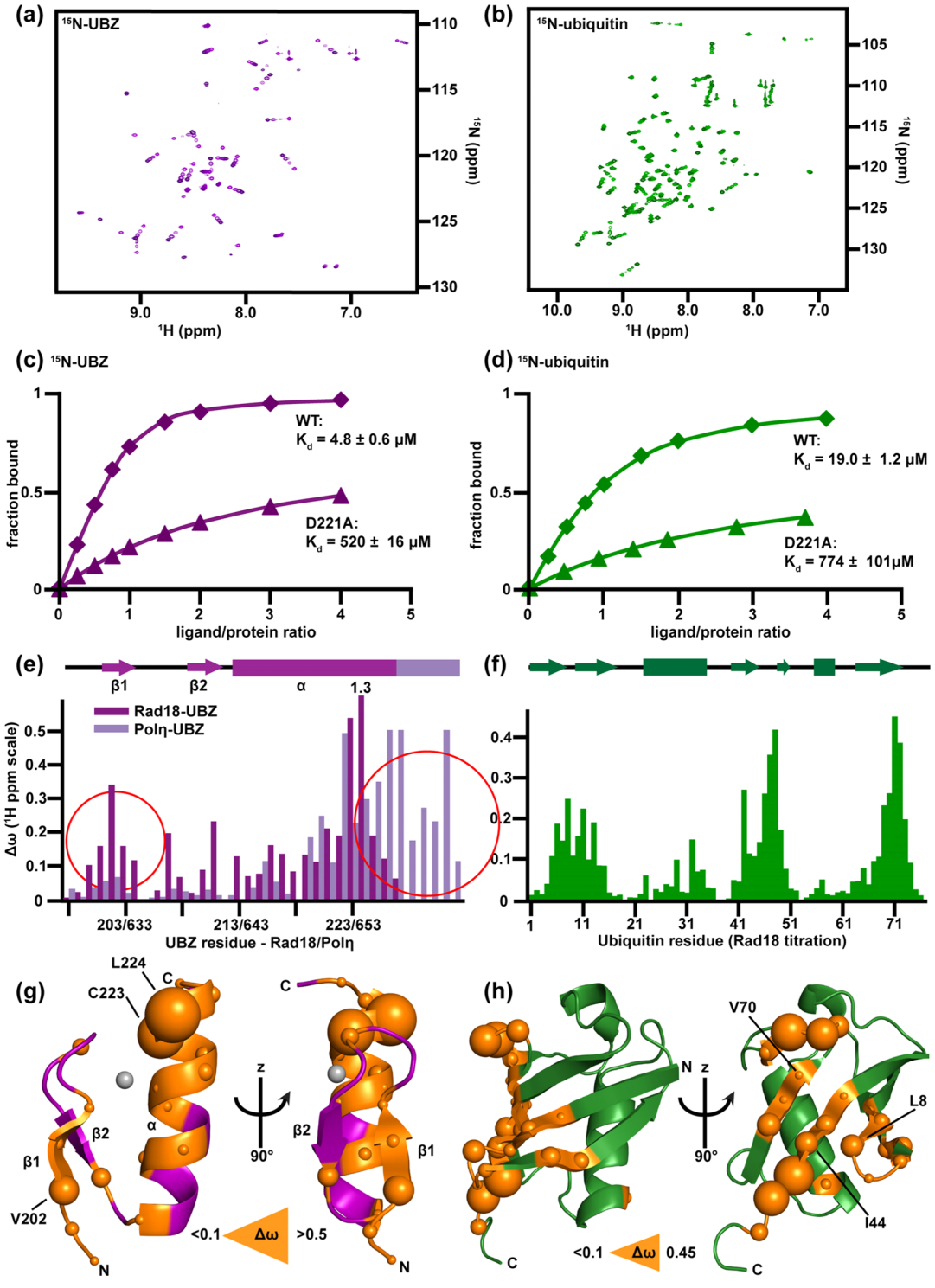

Figure 3. (a) Series of $^{1}H-^{15}N$ HSQC spectra recorded during titration of ^{15}N-labeled Rad18-UBZ domain with increasing amounts of unlabeled ubiquitin. (b) Reciprocal series of $^{1}H-^{15}N$ HSQC spectra collected during titration of ^{15}N-labeled ubiquitin with increasing amounts of unlabeled Rad18-UBZ domain. (c) Normalized cumulative chemical shift changes (see Experimental Procedures) for the backbone amide groups of the ^{15}N-labeled wild-type (diamonds) and D221A (triangles) Rad18-UBZ domain upon titration with the unlabeled ubiquitin and their best fits to a two-state binding model (lines). (d) Reciprocal cumulative chemical shift changes upon titration of ^{15}N-labeled ubiquitin with the unlabeled wild-type (diamonds) and D221A (triangles) Rad18-UBZ domain. Note that the D221A titration profile in panel d includes two additional points at a ligand:protein ratio of up to 7:1 that were omitted to improve the presentation; these points fall directly on the best-fit curve. (e) Per-residue backbone amide chemical shift differences between the bound and free ^{15}N-labeled Rad18-UBZ domain (magenta) and the bound and free ^{15}N-labeled Pol*η*-UBZ domain[35] (light purple) upon titration with unlabeled ubiquitin. Red circles highlight the difference in the location of chemical shift perturbations induced by ubiquitin binding between the Rad18- and Pol*η*-UBZ domains. (f) Per-residue chemical shift differences between bound and free ^{15}N-labeled ubiquitin upon titration with unlabeled Rad18-UBZ. (g and h) Binding-induced chemical shift perturbations for the backbone amide groups (plots e and f) mapped onto the structures of the Rad18-UBZ domain (g) and ubiquitin (h). The radii of the orange spheres are proportional to the chemical shift differences between bound and free forms.

dx.doi.org/10.1021/bi500823h | *Biochemistry* 2014, 53, 5895−5906

coordinate zinc should be interpreted in the context of a model in which the Rad18-UBZ domain is locally unfolded. In accordance with this, we were unable to purify a sufficient quantity of the C207F Rad18-UBZ domain for NMR titration experiments because of the instability of this construct.

Previous works investigating the UBZ domain−ubiquitin interaction identified a conserved aspartate residue located between the third and fourth zinc-coordinating residues [-C-X-X-C-$(X)_n$-(C/H)-X-**D**-X-(C/H)-], which is critical for the ubiquitin binding activity of UBZ domains.[25,33−35] Thus, GST-ubiquitin is unable to pull down the Rad18 variant harboring the D221A mutation *in vitro*.[34] Unlike WT Rad18, the D221A mutant (like C207F) does not coprecipitate with ubiquitinated H2A after treatment with ionizing radiation and does not form ionizing radiation-induced foci at DSB sites *in vivo*.[33] The equivalent mutation in the Polη-UBZ domain, D652A, abrogates the ubiquitin binding activity of Polη and similarly prevents localization of Polη to UV-induced foci.[25]

We have examined the ubiquitin binding activity of the ^{15}N-labeled D221A Rad18-UBZ domain (residues 198−227) using NMR titration experiments performed in a manner similar to the WT domain (Figure 3c,d). A ^{1}H−^{15}N HSQC spectrum of the D221A Rad18-UBZ domain (data not shown) displays good peak dispersion and little deviation in peak position from the WT, indicating that the D221A mutant remains properly folded. The titration data, however, reveal that the ubiquitin binding affinity for the D221A mutant (K_d = 520−774 μM) is ∼2 orders of magnitude weaker than that of the WT Rad18-UBZ domain (Figure 3c,d). Taken together, these results suggest that the D221A mutation affects formation of the UBZ domain−ubiquitin complex by disrupting an intermolecular interaction rather than by local unfolding of the domain (as in C207F). Therefore, D221A represents a Rad18 mutant that specifically knocks out ubiquitin binding while preserving the structure of the domain and its interactions with other putative partners that do not involve the mutation site.

Chemical Shift Mapping of the Rad18-UBZ Domain−Ubiquitin Binding Interface. With the NMR assignments completed for both partners, binding-induced chemical shift perturbations can be assessed on a per-residue basis to map the interface of the Rad18-UBZ domain−ubiquitin complex. Panels e and f of Figure 3 show chemical shift differences between the bound and free states for the backbone amide groups plotted versus residue number of the Rad18-UBZ domain (plot e, magenta) and ubiquitin (plot f) obtained from the analysis of NMR titration data. Panels g and h of Figure 3 show the measured chemical shift changes mapped onto the structures of the Rad18-UBZ domain (plot g) and ubiquitin (plot h) outlining the binding sites. Figure 3e (light purple) also illustrates the previously reported chemical shift perturbations induced by ubiquitin binding for the backbone amide groups of the Polη-UBZ domain.[35]

As expected, the Rad18-UBZ domain interacts with the conserved hydrophobic surface of the ubiquitin β-sheet centered at L8/I44/V70, which is also utilized by many other ubiquitin-binding domains and motifs (Figure 3f,h). The greatest chemical shift perturbations in the Rad18-UBZ domain upon ubiquitin binding occur in residues V202, C223, and L224 (Figure 3e,g), which map to strand β1 (V202) and the corresponding side face of the α-helix (C223 and L224) (Figure 3g). These secondary structure elements form a hydrophobic patch on the UBZ domain surface highlighted in Figure 2c. These data suggest a unique mode of ubiquitin recognition by the Rad18-UBZ domain in which both the α-helix and strand β1 contribute residues to the binding interface. This mode is distinctly different from that observed for the Polη-UBZ domain−ubiquitin interaction[35] in which the binding-induced chemical shift perturbations are located solely on the outer face of the helix with little change elsewhere in the UBZ domain (Figure 3e). Additionally, the Polη-UBZ domain forms an α-helix longer than that of the Rad18-UBZ domain, with chemical shifts for these extra C-terminal residues affected by ubiquitin binding (Figure 3e). The disparity in the location of the chemical shift perturbations between the Rad18-UBZ and Polη-UBZ domains indicates that Rad18-type UBZ domains utilize a novel interface for ubiquitin binding distinct from that of the Polη-UBZ domain.

The NMR Structure of the RAD18-UBZ Domain−Ubiquitin Complex Shows a Novel Binding Mode. Figure 4a (left) shows the NMR structure of the human Rad18-UBZ domain in complex with ubiquitin. For comparison, Figure 4b shows a model of the Polη-UBZ domain−ubiquitin complex generated as described by Bomar et al.[35] Similar to the structure of the free Rad18-UBZ domain (Figure 2a), the structure of the Rad18-UBZ domain−ubiquitin complex agrees well with the input experimental restraints and displays minimal violations from idealized molecular geometry (Table 1). Individually, neither the Rad18-UBZ domain nor ubiquitin undergoes significant conformational rearrangements upon complex formation, displaying an all-atom rmsd (calculated in PyMol[58]) between the free and bound forms of 0.97 Å for the UBZ over residues 200−225 and 1.2 Å for ubiquitin over all residues (calculated against a 1.8 Å resolution X-ray structure of ubiquitin,[59] PDB entry 1UBQ).

In agreement with the binding-induced chemical shift perturbations (Figure 3g,h), the interface of the Rad18-UBZ domain−ubiquitin complex is centered around the hydrophobic side chains of V202, P205, V206, I216, L220, and L224 in the UBZ domain and L8, I44, and V70 in ubiquitin (Figure 4a). Among the binding site residues in the UBZ domain, V202, P205, and V206 are located in strand β1 and the β1−β2 loop, while I216, N217, L220, D221, and L224 are located on the corresponding side face of the α-helix. Together, these residues form a large hydrophobic patch on the UBZ domain surface (Figure 2c). To further illustrate that strand β1 is indeed found at the UBZ domain−ubiquitin interface, Figure 4c shows reciprocal intermolecular NOE correlations in the two ^{13}C-edited, ^{13}C,^{15}N-filtered NOESY-HSQC spectra[41] between the $^{1}H^{\beta}$ proton of V202 from strand β1 of the UBZ domain and the $^{1}H^{\beta}$ protons of L8 in ubiquitin. Additional strips from the ^{13}C-edited, ^{13}C,^{15}N-filtered NOESY-HSQC spectra can be found in Figure S1 of the Supporting Information.

On the other side, ubiquitin interacts with the Rad18-UBZ domain via the canonical hydrophobic patch centered on L8/I44/V70 (Figure 4a, left). In addition, R42 and R72 on the rim of the ubiquitin−UBZ domain interface are located in the proximity of D221 and N217 from the UBZ α-helix, forming almost what appears to be an ionic cluster (Figure 4a, right). Two of these residues, D221 in the Rad18-UBZ domain and R42 in ubiquitin, form an intermolecular salt bridge. The D221/R42 salt bridge plays a critical role in stabilization of the Rad18-UBZ domain−ubiquitin complex, as suggested by a decrease of 2 orders of magnitude in the binding affinity of ubiquitin for the D221A Rad18-UBZ domain mutant compared to the WT (Figure 3c,d). Thus, the structure of the UBZ domain−ubiquitin complex provides the molecular basis for the

dx.doi.org/10.1021/bi500823h | *Biochemistry* 2014, 53, 5895−5906

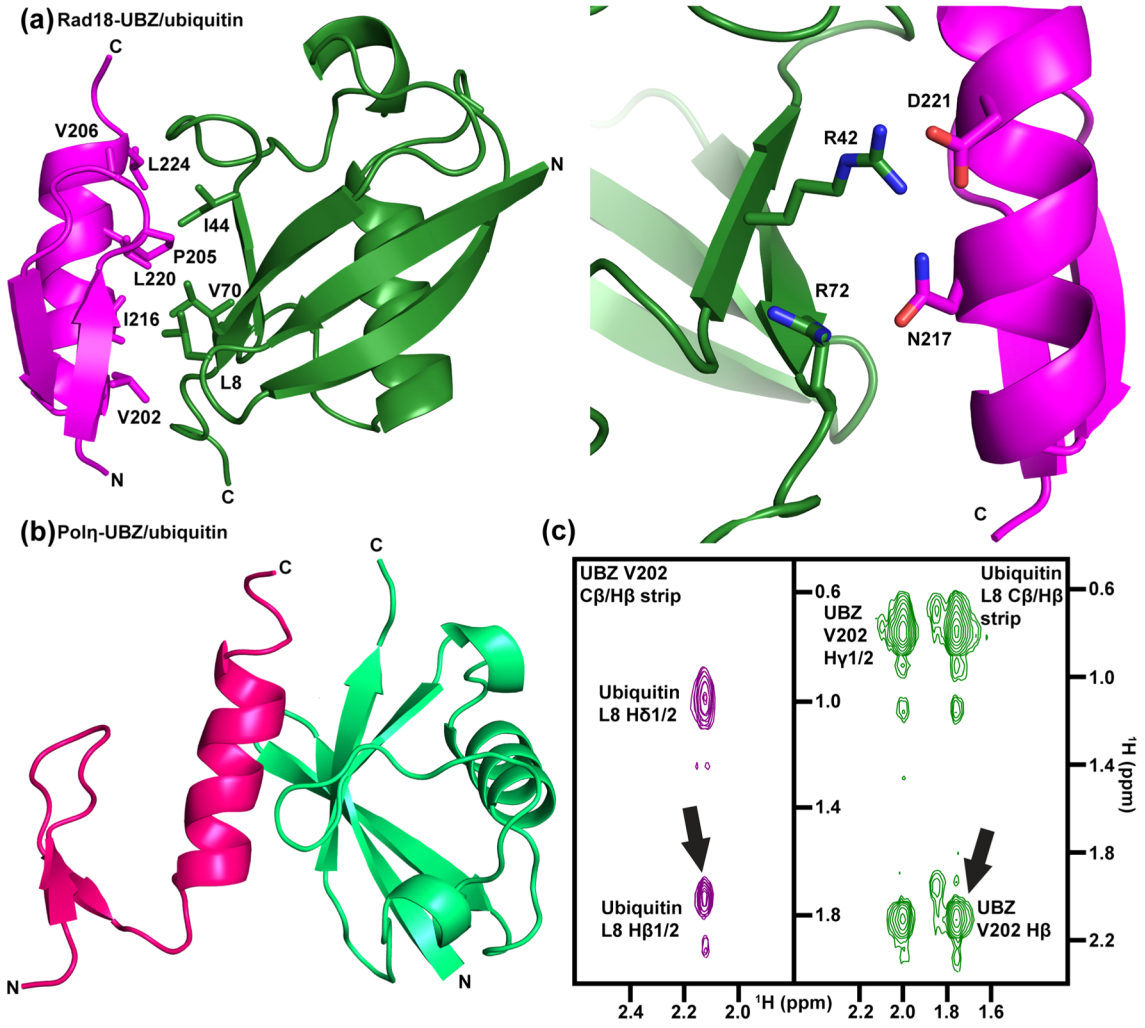

Figure 4. (a) NMR structure of the Rad18-UBZ domain−ubiquitin complex with side chains of V202, P205, V206, I216, L220, and L224 on the UBZ domain and L8, I44, and V70 on ubiquitin at the binding interface displayed (left). Close-up view of the intermolecular interaction between D221 and N217 of the Rad18-UBZ domain and R42 and R72 of ubiquitin (right). (b) Model of the Polη-UBZ domain−ubiquitin complex re-created as described by Bomar et al.[35] (c) Strips from the ^{13}C-edited, ^{13}C,^{15}N-filtered NOESY-HSQC spectra[41] of the ^{15}N/^{13}C-labeled Rad18-UBZ domain in complex with unlabeled ubiquitin (left) and ^{15}N- and ^{13}C-labeled ubiquitin in complex with the unlabeled Rad18-UBZ domain (right) showing reciprocal NOE correlations between H^{β} of V202 on the UBZ domain and H^{β} of L8 on ubiquitin.

use of the D221A UBZ as a ubiquitin-binding knockout mutant in previous *in vitro* and *in vivo* studies.[33,34] Interestingly, ionic interactions involving R42 and R72 are often found on the rims of ubiquitin interfaces with its interaction partners, given the proximity of these residues to the L8/I44/V70 hydrophobic face. For instance, salt bridges formed by these residues were also found in ubiquitin complexes with the protein S5a[60] and the ubiquitin-interaction motif (UIM) from Hrs.[61]

Recently, Bomar et al. determined the spatial structure of the UBZ domain from the TLS DNA polymerase Polη,[35] which adopts a fold very similar to that of the Rad18-UBZ domain (Figure 2b). This work also reported a structural model of the Polη-UBZ domain−ubiquitin complex re-created in Figure 4b.[35] The model was built on the basis of NMR chemical shift perturbations and spin-labeling data, taking advantage of the sequence and structural conservation between the Polη-UBZ domain and a bovine Rabex-5 MIU/IUIM fragment in complex with ubiquitin.[37] In striking contrast to the Rad18-UBZ domain−ubiquitin complex in which both strand β1 and the α-helix are involved in interaction (Figure 4a), the model of the Polη-UBZ domain−ubiquitin complex reveals that the ubiquitin-binding interface is located on the outside of the UBZ domain α-helix with no role for strand β1[35] (Figure 4b). Note that the surface of the helix and strand β1 utilized by the Rad18-UBZ domain for ubiquitin binding is more acidic in the Polη-UBZ domain (Figure 2c). The Rad18-UBZ and Polη-UBZ domains also bind ubiquitin in different orientations, where the UBZ α-helix is rotated by about 90° relative to the ubiquitin surface (Figure 4a,b). Furthermore, the conserved aspartates, D221 in Rad18 and D652 in Polη between the final two zinc-coordinating residues [-(C/H)-X-**D**-X-C-], appear to fulfill different roles: D221 in Rad18 forms a salt bridge with the side chain of R42 on ubiquitin, while D652 in Polη interacts with the backbone of A46 and G47 on ubiquitin.[35] Therefore, the models of the complexes of the Rad18-UBZ and Polη-UBZ domains with ubiquitin shown in Figure 4 define two distinctly different ubiquitin-binding modes for these structurally similar domains.

Distinction between Type 3 Polη-like and Type 4 Rad18-like UBZ Domains. Figure 5a shows a sequence alignment of Rad18-UBZ domains from different species (top) and UBZ domains from different human proteins (bottom).

dx.doi.org/10.1021/bi500823h | *Biochemistry* 2014, 53, 5895−5906

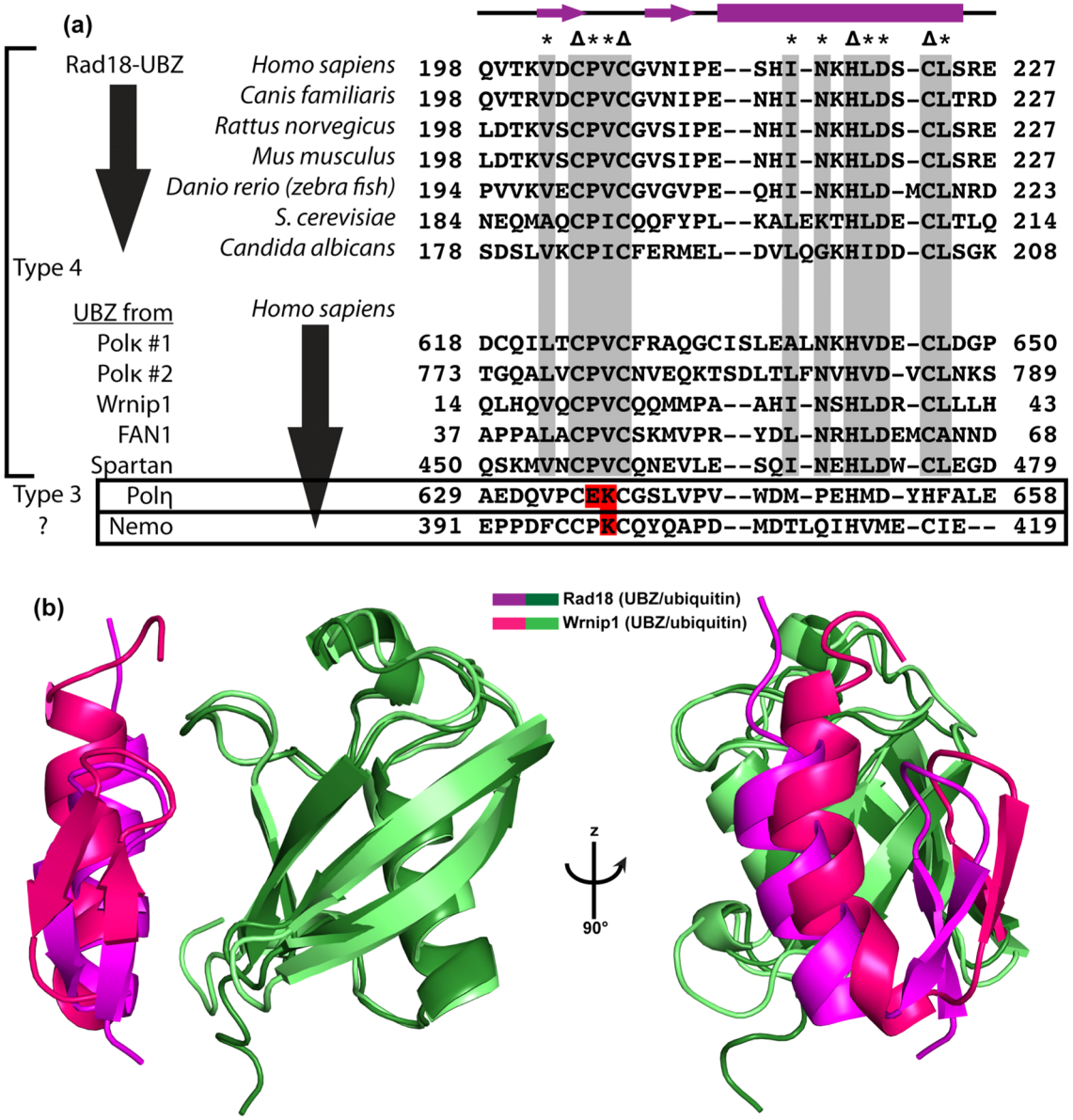

Figure 5. (a) Alignment of the sequences of Rad18-UBZ domains from different species (top) and UBZ domains from different human proteins (bottom). Zinc-coordinating residues are marked with uppercase deltas. Residues that are at the binding interface are marked with asterisks. Residues that are conserved by type are colored gray. The initial alignment was performed in ClustalW[65] and then manually edited to ensure alignment of the last zinc-coordinating residue. All UBZ domains shown except the ones from Pol*η* and NEMO (two last lines) are type 4 C_2HC UBZ4s, while the Pol*η*-UBZ domain belongs to type 3 C_2H_2 UBZ3. (b) Superposition of the Rad18-UBZ domain−ubiquitin complex with the structure of the Wrnip1-UBZ domain−ubiquitin complex (PDB entry 3VHT) where the UBZs are colored magenta and red and ubiquitin is colored two shades of green.

Zinc-coordinating residues are aligned and are marked with uppercase deltas. Residues at or near the Rad18-UBZ domain−ubiquitin binding interface are marked with asterisks and are highly conserved by type (gray) both in Rad18-UBZ domains from different species and in most UBZ domains from other human proteins. This is expected, because residues at a binding interface are typically more conserved with respect to other surface-exposed residues.[62]

The sequence conservation is weaker between UBZ domains from Rad18 and Pol*η*. Previously, on the basis of differences in their primary sequence, UBZ domains in DDR-related proteins were divided into subgroups, type 3 C_2H_2 UBZ3 (Pol*η*-like) and type 4 C_2HC UBZ4 (Rad18-like).[14,25,34] Beyond the obvious difference in zinc-coordinating residues, the physical manifestation of this disparity has not been apparent. In fact, both Pol*η*-UBZ3 and Rad18-UBZ4 domains are classical $\beta1-\beta2-\alpha$ domains containing a conserved aspartate residue involved in ubiquitin binding (D652 in Pol*η* and D221 in Rad18). Therefore, most previous publications simply refer to the "UBZ" class of ubiquitin-binding domains with no mention of any delineation.

The sequence alignment shown in Figure 5a and the structures of the complexes of the Pol*η*-UBZ3 and Rad18-UBZ4 domains with ubiquitin (Figure 4a,b) suggest that, while sharing a conserved aspartate residue, the UBZ3 and UBZ4 domains differ in other residues contributing to ubiquitin binding. The only representative of the type 3 domains, the Pol*η*-UBZ3, has a stretch of charged amino acids (C-**E**-**K**-C) in

dx.doi.org/10.1021/bi500823h | *Biochemistry* 2014, 53, 5895−5906

place of the invariant hydrophobic C-**P**-**V**/**I**-C sequence (residues 204−207 from strand β1 and the β1−β2 loop of the Rad18-UBZ domain) in the ubiquitin-binding site of UBZ4s (Figure 5a). The glutamate E636 determines the acidic nature of the surface of the Polη-UBZ3 domain formed by strand β1 and the α-helix (Figure 2c), while the following lysine K637 folds back into the structure and forms a salt bridge with E658, stabilizing the longer α-helix.[35] The conservation among I216, N217, L220, and L224 from the Rad18-UBZ4 domain-binding site for ubiquitin and the equivalent residues from the Polη-UBZ3 domain is also weak, providing additional evidence that the ubiquitin-binding mode of the Polη-UBZ domain is different from that of the UBZ4 domains.

The sequence alignment of the C_2HC UBZ domain from the protein NEMO (Figure 5a, last line) does not allow its classification into either type 3 or type 4. Previous work has indicated that ubiquitin binding by this domain occurs on the outside of the α-helix, similar to the Polη-type UBZ3 domains.[38] However, because the critical A655, L659, and Q660 from Polη and the Rabex MIU/IUIM motif[37] have no equivalent residues in NEMO, and because the α-helix is shorter in the NEMO-UBZ domain (Figure 5a; E419 is the C-terminal residue), this UBZ domain may itself be unique.

Interestingly, the unique ubiquitin-binding mode of the Rad18-UBZ4 domain with the ubiquitin-binding site formed by strand β1 and the α-helix (Figure 4a) is confirmed by an unpublished structure of a related type 4 UBZ domain from the protein Wrnip1 [PDB entry 3VHT (Figure 5a, line 10)]. This crystal structure, determined at 2.4 Å resolution, contains a GFP fusion protein of the Wrnip1-UBZ4 domain in complex with ubiquitin. Figure 5b shows a structural alignment of the Rad18-UBZ4 domain−ubiquitin and Wrnip1-UBZ4 domain−ubiquitin complexes confirming the conservation of binding modes among UBZ4 domains with strand β1 in the Wrnip1-UBZ domain located at the ubiquitin binding interface (the hallmark of the UBZ4 class). Sequence alignment (Figure 5a) shows that all residues in the Rad18-UBZ4 domain binding interface and hydrophobic core are completely conserved in the Wrnip1-UBZ domain, including V202, C204−C207, I216, N217, L220, D221, and L224. These residues define the UBZ4-type sequence with a binding mode unique compared to that of the Polη-UBZ domain. Additionally, the D221/R42 salt bridge is also conserved, with D37 being the equivalent in Wrnip1.

Taken together, the previous definitions of the UBZ3 and UBZ4 domains[14,25,34] can now be refined to include structural information, although the biological implications of the difference in binding mode are not immediately evident. Both types of UBZ domains seem to have similar roles in subcellular localization, because their knockout prevents the recruitment of protein to DNA repair factories after exposure to UV light or ionizing radiation.[11,25,63] However, there is no discernible pattern in the literature that might suggest specificity of UBZ3 versus UBZ4 domains in response to certain types of damage. Presumably, the difference in ubiquitin recognition modes of the UBZ3 and UBZ4 domains is related to a unique role played by Polη in translesion synthesis (TLS) because it is the only known protein with a UBZ3 domain while UBZ4 domains are numerous. The presented structural comparison of the UBZ3 and UBZ4 domains thus provides context for further studies to delineate their differential functions in the DNA damage response.

CONCLUDING REMARKS

In summary, we have presented the NMR structure of the human Rad18-UBZ domain, both isolated and in complex with ubiquitin, and have characterized the interaction of the WT Rad18-UBZ domain and its point mutants with ubiquitin by NMR titration experiments. The results show that the Rad18-UBZ domain has the canonical β1−β2−α topology also found in the UBZ domain from Polη[35] and DNA-binding zinc fingers.[36] To our surprise, the ubiquitin-binding interface of the Rad18-UBZ domain is different from that observed in the model of the Polη-UBZ domain−ubiquitin complex generated using NMR chemical shift perturbations and spin-labeling.[35] Sequence alignment of UBZ domains and the location of NMR chemical shift perturbations in the Polη- and Rad18-UBZ domains upon ubiquitin binding suggest that the two domains have nearly identical structures but bind ubiquitin with different modes. Previous studies proposed categorization of UBZ domains in proteins linked to the DNA damage response into two classes: Polη-like type 3 (UBZ3) and Rad18-like type 4 (UBZ4).[14,25,34] The structure of the Rad18-UBZ domain−ubiquitin complex determined here and the sequence alignment of UBZ domains provide a clear basis for this delineation, suggesting the possibility of differences in the functional roles of these two domain types.

ASSOCIATED CONTENT

Supporting Information

A selection of strips from the ^{13}C-edited, ^{13}C,^{15}N-filtered NOESY-HSQC spectra with intermolecular NOEs (Figure S1). This material is available free of charge via the Internet at http://pubs.acs.org.

Accession Codes

Atomic coordinates for the free Rad18 UBZ domain and the UBZ domain−ubiquitin complex have been deposited in the Protein Data Bank as entries 2MRF and 2MRE, respectively. Backbone and side-chain chemical shifts of the UBZ domain and the UBZ domain−ubiquitin complex have been deposited in the BMRB as entries 25071 and 25070, respectively.

AUTHOR INFORMATION

Corresponding Author

*E-mail: korzhniev@uchc.edu. Phone: (860) 679-2849. Fax: (860) 679-3408.

Funding

This work was supported by University of Connecticut Health Center startup funds and a CICATS pilot grant to D.M.K. and by a CT DPH biomedical research award and CT stem cell research grant to I.B.

Notes

The authors declare no competing financial interest.

ACKNOWLEDGMENTS

We thank Mark Maciejewski (University of Connecticut Health Center) for help collecting data, Karlene Cimprich and Michelle Zeman (Stanford University, Stanford, CA) for providing plasmids and helpful discussions, and Pei Zhou (Duke University, Durham, NC) for providing the NMR chemical shift perturbation data for the Polη-UBZ domain−ubiquitin titration.

■ ABBREVIATIONS

3D, three-dimensional; DDR, DNA damage response; BMRB, Biological Magnetic Resonance Bank; DSB, double-strand break (DNA); HRR, homologous recombination repair; HSQC, heteronuclear single-quantum correlation spectroscopy; MIU/IUIM, motif interacting with ubiquitin/inverted ubiquitin-interacting motif; NMR, nuclear magnetic resonance; NOESY, nuclear Overhauser effect spectroscopy; PCNA, proliferating cell nuclear antigen; PDB, Protein Data Bank; rmsd, root-mean-square deviation; TLS, translesion synthesis; UBM, ubiquitin-binding motif; UBZ, ubiquitin-binding zinc finger; UIM, ubiquitin-interacting motif; UV, ultraviolet.

■ REFERENCES

(1) Friedberg, E. C., Walker, G. C., Siede, W., Wood, R. D., Schultz, R. A., and Ellenberger, T. (2005) *DNA Repair and Mutagenesis*, 2nd ed., ASM Press, Washington, DC.

(2) Chang, D. J., and Cimprich, K. A. (2009) DNA damage tolerance: When it's OK to make mistakes. *Nat. Chem. Biol. 5*, 82−90.

(3) Mailand, N., Bekker-Jensen, S., Faustrup, H., Melander, F., Bartek, J., Lukas, C., and Lukas, J. (2007) RNF8 Ubiquitylates Histones at DNA Double-Strand Breaks and Promotes Assembly of Repair Proteins. *Cell 131*, 887−900.

(4) Branzei, D., and Foiani, M. (2008) Regulation of DNA repair throughout the cell cycle. *Nat. Rev. Mol. Cell Biol. 9*, 297−308.

(5) Waters, L. S., Minesinger, B. K., Wiltrout, M. E., D'Souza, S., Woodruff, R. V., and Walker, G. C. (2009) Eukaryotic Translesion Polymerases and Their Roles and Regulation in DNA Damage Tolerance. *Microbiol. Mol. Biol. Rev. 73*, 134−154.

(6) Hoege, C., Pfander, B., Moldovan, G.-L., Pyrowolakis, G., and Jentsch, S. (2002) RAD6-dependent DNA repair is linked to modification of PCNA by ubiquitin and SUMO. *Nature 419*, 135−141.

(7) Harper, J. W., and Elledge, S. J. (2007) The DNA Damage Response: Ten Years After. *Mol. Cell 28*, 739−745.

(8) Ciccia, A., and Elledge, S. J. (2010) The DNA Damage Response: Making It Safe to Play with Knives. *Mol. Cell 40*, 179−204.

(9) Pickart, C. M., and Fushman, D. (2004) Polyubiquitin chains: Polymeric protein signals. *Curr. Opin. Chem. Biol. 8*, 610−616.

(10) Bergink, S., and Jentsch, S. (2009) Principles of ubiquitin and SUMO modifications in DNA repair. *Nature 458*, 461−467.

(11) Huang, J., Huen, M. S. Y., Kim, H., Leung, C. C. Y., Glover, J. N. M., Yu, X., and Chen, J. (2009) RAD18 transmits DNA damage signalling to elicit homologous recombination repair. *Nat. Cell Biol. 11*, 592−603.

(12) Al-Hakim, A., Escribano-Diaz, C., Landry, M.-C., O'Donnell, L., Panier, S., Szilard, R. K., and Durocher, D. (2010) The ubiquitous role of ubiquitin in the DNA damage response. *DNA Repair 9*, 1229−1240.

(13) Huang, T. T., and D'Andrea, A. D. (2006) Regulation of DNA repair by ubiquitylation. *Nat. Rev. Mol. Cell Biol. 7*, 323−334.

(14) Hofmann, K. (2009) Ubiquitin-binding domains and their role in the DNA damage response. *DNA Repair 8*, 544−556.

(15) Sale, J. E., Lehmann, A. R., and Woodgate, R. (2012) Y-family DNA polymerases and their role in tolerance of cellular DNA damage. *Nat. Rev. Mol. Cell Biol. 13*, 141−152.

(16) Guo, C., Kosarek-Stancel, J. N., Tang, T.-S., and Friedberg, E. (2009) Y-family DNA polymerases in mammalian cells. *Cell. Mol. Life Sci. 66*, 2363−2381.

(17) Goodman, M. F. (2002) Error-prone Repair DNA Polymerases in Prokaryotes and Eukaryotes. *Annu. Rev. Biochem. 71*, 17−50.

(18) Prakash, S., Johnson, R. E., and Prakash, L. (2005) Eukaryotic Translesion Synthesis DNA Polymermases: Specificity of Structure and Function. *Annu. Rev. Biochem. 74*, 317−353.

(19) Lehmann, A. R., Niimi, A., Ogi, T., Brown, S., Sabbioneda, S., Wing, J. F., Kannouche, P. L., and Green, C. M. (2007) Translesion synthesis: Y-family polymerases and the polymerase switch. *DNA Repair 6*, 891−899.

(20) Trincao, J., Johnson, R. E., Escalante, C. R., Prakash, S., Prakash, L., and Aggarwal, A. K. (2001) Structure of the Catalytic Core of *S. cerevisiae* DNA Polymerase η: Implications for Translesion DNA Synthesis. *Mol. Cell 8*, 417−426.

(21) Kunkel, T. A. (2004) DNA Replication Fidelity. *J. Biol. Chem. 279*, 16895−16898.

(22) Xiao, W., Chow, B. L., Broomfield, S., and Hanna, M. (2000) The *Saccharomyces cerevisiae* RAD6 Group Is Composed of an Error-Prone and Two Error-Free Postreplication Repair Pathways. *Genetics 155*, 1633−1641.

(23) Moldovan, G.-L., Pfander, B., and Jentsch, S. (2007) PCNA, the Maestro of the Replication Fork. *Cell 129*, 665−679.

(24) Unk, I., Hajdú, I., Blastyák, A., and Haracska, L. (2010) Role of yeast Rad5 and its human orthologs, HLTF and SHPRH in DNA damage tolerance. *DNA Repair 9*, 257−267.

(25) Bienko, M., Green, C. M., Crosetto, N., Rudolf, F., Zapart, G., Coull, B., Kannouche, P., Wider, G., Peter, M., Lehmann, A. R., Hofmann, K., and Dikic, I. (2005) Ubiquitin-Binding Domains in Y-Family Polymerases Regulate Translesion Synthesis. *Science 310*, 1821−1824.

(26) Dikic, I., Wakatsuki, S., and Walters, K. J. (2009) Ubiquitin-binding domains: From structures to functions. *Nat. Rev. Mol. Cell Biol. 10*, 659−671.

(27) Notenboom, V., Hibbert, R. G., van Rossum-Fikkert, S. E., Olsen, J. V., Mann, M., and Sixma, T. K. (2007) Functional characterization of Rad18 domains for Rad6, ubiquitin, DNA binding and PCNA modification. *Nucleic Acids Res. 35*, 5819−5830.

(28) Kannouche, P. L., Wing, J., and Lehmann, A. R. (2004) Interaction of Human DNA Polymerase η with Monoubiquitinated PCNA: A Possible Mechanism for the Polymerase Switch in Response to DNA Damage. *Mol. Cell 14*, 491−500.

(29) Watanabe, K., Tateishi, S., Kawasuji, M., Tsurimoto, T., Inoue, H., and Yamaizumi, M. (2004) Rad18 guides polη to replication stalling sites through physical interaction and PCNA monoubiquitination. *EMBO J. 23*, 3886−3896.

(30) Miyase, S., Tateishi, S., Watanabe, K., Tomita, K., Suzuki, K., Inoue, H., and Yamaizumi, M. (2005) Differential Regulation of Rad18 through Rad6-dependent Mono- and Polyubiquitination. *J. Biol. Chem. 280*, 515−524.

(31) Masuda, Y., Suzuki, M., Kawai, H., Suzuki, F., and Kamiya, K. (2012) Asymmetric nature of two subunits of RAD18, a RING-type ubiquitin ligase E3, in the human RAD6A,RAD18 ternary complex. *Nucleic Acids Res. 40*, 1065−1076.

(32) Watanabe, K., Iwabuchi, K., Sun, J., Tsuji, Y., Tani, T., Tokunaga, K., Date, T., Hashimoto, M., Yamaizumi, M., and Tateishi, S. (2009) RAD18 promotes DNA double-strand break repair during G1 phase through chromatin retention of 53BP1. *Nucleic Acids Res. 37*, 2176−2193.

(33) Inagaki, A., Sleddens-Linkels, E., van Cappellen, W. A., Hibbert, R. G., Sixma, T. K., Hoeijmakers, J. H. J., Grootegoed, J. A., and Baarends, W. M. (2011) Human RAD18 Interacts with Ubiquitylated Chromatin Components and Facilitates RAD9 Recruitment to DNA Double Strand Breaks. *PLoS One 6*, e23155.

(34) Crosetto, N., Bienko, M., Hibbert, R. G., Perica, T., Ambrogio, C., Kensche, T., Hofmann, K., Sixma, T. K., and Dikic, I. (2008) Human Wrnip1 Is Localized in Replication Factories in a Ubiquitin-binding Zinc Finger-dependent Manner. *J. Biol. Chem. 283*, 35173−35185.

(35) Bomar, M. G., Pai, M.-T., Tzeng, S.-R., Li, S. S.-C., and Zhou, P. (2007) Structure of the ubiquitin-binding zinc finger domain of human DNA Y-polymerase η. *EMBO Rep. 8*, 247−251.

(36) Lee, M. S., Gippert, G. P., Soman, K. V., Case, D. A., and Wright, P. E. (1989) Three-dimensional solution structure of a single zinc finger DNA-binding domain. *Science 245*, 635−637.

(37) Lee, S., Tsai, Y. C., Mattera, R., Smith, W. J., Kostelansky, M. S., Weissman, A. M., Bonifacino, J. S., and Hurley, J. H. (2006) Structural basis for ubiquitin recognition and autoubiquitination by Rabex-5. *Nat. Struct. Mol. Biol. 13*, 264−271.

(38) Cordier, F., Grubisha, O., Traincard, F., Véron, M., Delepierre, M., and Agou, F. (2009) The Zinc Finger of NEMO Is a Functional Ubiquitin-binding Domain. *J. Biol. Chem. 284*, 2902−2907.
(39) Ho, S. N., Hunt, H. D., Horton, R. M., Pullen, J. K., and Pease, L. R. (1989) Site-directed mutagenesis by overlap extension using the polymerase chain reaction. *Gene 77*, 51−59.
(40) Sattler, M., Schleucher, J., and Griesinger, C. (1999) Heteronuclear multidimensional NMR experiments for the structure determination of proteins in solution employing pulsed field gradients. *Prog. Nucl. Magn. Reson. Spectrosc. 34*, 93−158.
(41) Zwahlen, C., Legault, P., Vincent, S. J. F., Greenblatt, J., Konrat, R., and Kay, L. E. (1997) Methods for Measurement of Intermolecular NOEs by Multinuclear NMR Spectroscopy: Application to a Bacteriophage λ N-Peptide/boxB RNA Complex. *J. Am. Chem. Soc. 119*, 6711−6721.
(42) Delaglio, F., Grzesiek, S., Vuister, G., Zhu, G., Pfeifer, J., and Bax, A. (1995) NMRPipe: A multidimensional spectral processing system based on UNIX pipes. *J. Biomol. NMR 6*, 277−293.
(43) Vranken, W. F., Boucher, W., Stevens, T. J., Fogh, R. H., Pajon, A., Llinas, M., Ulrich, E. L., Markley, J. L., Ionides, J., and Laue, E. D. (2005) The CCPN data model for NMR spectroscopy: Development of a software pipeline. *Proteins: Struct., Funct., Bioinf. 59*, 687−696.
(44) Farrow, N. A., Muhandiram, R., Singer, A. U., Pascal, S. M., Kay, C. M., Gish, G., Shoelson, S. E., Pawson, T., Forman-Kay, J. D., and Kay, L. E. (1994) Backbone dynamics of a free and phosphopeptide-complexed Src homology 2 domain studied by ^{15}N NMR relaxation. *Biochemistry 33*, 5984−6003.
(45) Güntert, P. (2004) Automated NMR Structure Calculation with CYANA. In *Protein NMR Techniques* (Downing, A. K., Ed.) pp 353−378, Humana Press, Totowa, NJ.
(46) Shen, Y., Delaglio, F., Cornilescu, G., and Bax, A. (2009) TALOS+: A hybrid method for predicting protein backbone torsion angles from NMR chemical shifts. *J. Biomol. NMR 44*, 213−223.
(47) Alberts, I. L., Nadassy, K., and Wodak, S. J. (1998) Analysis of zinc binding sites in protein crystal structures. *Protein Sci. 7*, 1700−1716.
(48) Brunger, A. T., Adams, P. D., Clore, G. M., DeLano, W. L., Gros, P., Grosse-Kunstleve, R. W., Jiang, J.-S., Kuszewski, J., Nilges, M., Pannu, N. S., Read, R. J., Rice, L. M., Simonson, T., and Warren, G. L. (1998) Crystallography & NMR System: A New Software Suite for Macromolecular Structure Determination. *Acta Crystallogr. D54*, 905−921.
(49) Deshaies, R. J., and Joazeiro, C. A. P. (2009) RING Domain E3 Ubiquitin Ligases. *Annu. Rev. Biochem. 78*, 399−434.
(50) Panier, S., Ichijima, Y., Fradet-Turcotte, A., Leung, C. C., Kaustov, L., Arrowsmith, C. H., and Durocher, D. (2012) Tandem Protein Interaction Modules Organize the Ubiquitin-Dependent Response to DNA Double-Strand Breaks. *Mol. Cell 47*, 383−395.
(51) Huang, A., Hibbert, R. G., de Jong, R. N., Das, D., Sixma, T. K., and Boelens, R. (2011) Symmetry and Asymmetry of the RING−RING Dimer of Rad18. *J. Mol. Biol. 410*, 424−435.
(52) Hibbert, R. G., Huang, A., Boelens, R., and Sixma, T. K. (2011) E3 ligase Rad18 promotes monoubiquitination rather than ubiquitin chain formation by E2 enzyme Rad6. *Proc. Natl. Acad. Sci. U.S.A. 108*, 5590−5595.
(53) Machado, L. F., Pustovalova, Y., Kile, A., Pozhidaeva, A., Cimprich, K., Almeida, F. L., Bezsonova, I., and Korzhnev, D. (2013) PHD domain from human SHPRH. *J. Biomol. NMR 56*, 393−399.
(54) Lee, M. S., Gottesfeld, J. M., and Wright, P. E. (1991) Zinc is required for folding and binding of a single zinc finger to DNA. *FEBS Lett. 279*, 289−294.
(55) Pascual, J., Martinez-Yamout, M., Dyson, H. J., and Wright, P. E. (2000) Structure of the PHD Zinc Finger from Human Williams-Beuren Syndrome Transcription Factor. *J. Mol. Biol. 304*, 723−729.
(56) Berjanskii, M. V., and Wishart, D. (2008) Application of the random coil index to studying protein flexibility. *J. Biomol. NMR 40*, 31−48.
(57) Berjanskii, M. V., and Wishart, D. S. (2005) A Simple Method To Predict Protein Flexibility Using Secondary Chemical Shifts. *J. Am. Chem. Soc. 127*, 14970−14971.
(58) *The PyMOL Molecular Graphics System*, version 1.5.0.4 Schrödinger, LLC, Portland, OR, http://www.pymol.org/.
(59) Vijay-Kumar, S., Bugg, C. E., and Cook, W. J. (1987) Structure of ubiquitin refined at 1.8 Å resolution. *J. Mol. Biol. 194*, 531−544.
(60) Wang, Q., Young, P., and Walters, K. J. (2005) Structure of S5a Bound to Monoubiquitin Provides a Model for Polyubiquitin Recognition. *J. Mol. Biol. 348*, 727−739.
(61) Hirano, S., Kawasaki, M., Ura, H., Kato, R., Raiborg, C., Stenmark, H., and Wakatsuki, S. (2006) Double-sided ubiquitin binding of Hrs-UIM in endosomal protein sorting. *Nat. Struct. Mol. Biol. 13*, 272−277.
(62) Guharoy, M., and Chakrabarti, P. (2005) Conservation and relative importance of residues across protein-protein interfaces. *Proc. Natl. Acad. Sci. U.S.A. 102*, 15447−15452.
(63) Plosky, B. S., Vidal, A. E., de Henestrosa, A. R. F., McLenigan, M. P., McDonald, J. P., Mead, S., and Woodgate, R. (2006) Controlling the subcellular localization of DNA polymerases ι and η via interactions with ubiquitin. *EMBO J. 25*, 2847−2855.
(64) Guex, N., and Peitsch, M. C. (1997) SWISS-MODEL and the Swiss-Pdb Viewer: An environment for comparative protein modeling. *Electrophoresis 18*, 2714−2723.
(65) Larkin, M. A., Blackshields, G., Brown, N. P., Chenna, R., McGettigan, P. A., McWilliam, H., Valentin, F., Wallace, I. M., Wilm, A., Lopez, R., Thompson, J. D., Gibson, T. J., and Higgins, D. G. (2007) Clustal W and Clustal X version 2.0. *Bioinformatics 23*, 2947−2948.
(66) Doreleijers, J., Sousa da Silva, A., Krieger, E., Nabuurs, S., Spronk, C. E. M., Stevens, T., Vranken, W., Vriend, G., and Vuister, G. (2012) CING: An integrated residue-based structure validation program suite. *J. Biomol. NMR 54*, 267−283.